Numerical simulations of the electrical transport characteristics of a Pt/n-GaN Schottky diode

Fayçal Bouzid[1,2*], Fortunato Pezzimenti[3], Lakhdar Dehimi[1,2,4], Mohamed L. Megherbi[1], and Francesco G. Della Corte[3]

[1] Laboratory of Metallic and Semiconductor Materials, University of Biskra, P.O. Box 145, Biskra 07000, Algeria
[2] Thin Films Development and Applications Unit UDCMA, Setif / Research Center in Industrial Technologies CRTI, P.O. Box 64, Cheraga 16014, Algeria
[3] DIIES - University of Reggio Calabria, Loc. Feo di Vito, Reggio Calabria I-89100, Italy
[4] Faculty of Science, University of Batna, Batna 05000, Algeria

[*] E-mail address: f.bouzid@crti.dz

In this paper, using a numerical simulator, we investigated the current-voltage characteristics of a Pt/n-GaN thin Schottky diode on the basis of the thermionic emission (TE) theory in the 300 to 500 K temperature range. During the simulations, the effect of different defect states within the n-GaN bulk with different densities and spatial locations is considered. The results show that the diode ideality factor and the threshold voltage decrease with increasing temperature, while at the same time, the zero-bias Schottky barrier height (Φ_{b0}) extracted from the forward current density-voltage (*J-V*) characteristics increases. The observed behaviors of the ideality factor and zero-bias barrier height are analyzed on the basis of spatial barrier height inhomogeneities at the Pt/GaN interface by assuming a Gaussian distribution (GD). The plot of apparent barrier height ($\Phi_{b,App}$) as a function of $q/2kT$ gives a straight line, where the mean zero-bias barrier height ($\overline{\Phi_{b0}}$) and the standard deviation (σ_0) are 1.48 eV and 0.047 V, respectively. The plot of the modified activation energy against q/kT gives an almost the same value of $\overline{\Phi_{b0}}$ and an effective Richardson constant A^* of 28.22 $Acm^{-2}K^{-2}$, which is very close to the theoretical value for n-type GaN/Pt contacts. As expected, the presence of defect states with different trap energy levels has a noticeable impact on the device electrical characteristics.

Japanese Journal of Applied Physics, n.56, pp. 94301, 2017.
https://doi.org/10.7567/jjap.56.094301
This Accepted Manuscript is available for reuse under a CC BY-NC-ND licence after the 12 month embargo period provided that all the terms of the licence are adhered to.

1. Introduction

Gallium nitride (GaN) is one of the most interesting semiconductor compounds well suited for operating in any application in which the environmental temperatures or level of radiation might damage conventional silicon (Si) or gallium arsenide (GaAs) electronics [1]. Compared with other materials, the most attractive properties of GaN are its wide-bandgap energy, high carrier saturation velocity, high thermal conductivity and stability, high breakdown electric field, and capability to form high-quality heterostructures with good transport properties [2]. In recent years, a great number of GaN-based devices, such as light-emitting diodes, laser diodes, photodetectors, and radiation detectors have been developed [3-5].

Schottky structures offer significant advantages over p-i-n ones both in terms of superior switching characteristics and reduced reverse recovery power losses [6]. Several studies on GaN Schottky diodes have been carried out using different metals such as platinum (Pt) [7-9], palladium (Pd) [7-9], gold (Au) [7,10,11], nickel (Ni) [7,9,12], chromium (Cr) [13], and titanium (Ti) [7,14]. In particular, Pt has a high work function, which makes it ideal for use as Schottky contacts on n-type GaN substrates. In fact, according to the Schottky-Mott model, the Schottky barrier height (SBH) is dependent on the metal work function and semiconductor electron affinity. Finally, Pt appears resistant to oxidation and corrosion [15].

In this paper, the current density-voltage (*J-V*) characteristics of a Pt/n-GaN Schottky diode are investigated in a wide range of temperatures by a careful simulation study, which is useful for evaluating different aspects of barrier formation and current transport mechanisms. The temperature dependences of SBH and ideality factor are interpreted on the basis of the thermionic emission (TE) theory and assuming a Gaussian distribution (GD) of SBH on the basis of the Tung [16] as well as Werner and Güttler [17] models.

The device is well suited for ultraviolet detection applications. With this purpose, the impact of the presence of shallow and deep acceptor trap energy levels in the GaN bulk with different densities of states is also investigated. A wide range of operating temperatures and exposure to high levels of radiation strongly affect the device performance and detection properties, generating charged defect centres [18,19].

2. Device structure

A schematic cross-sectional view of the Pt/n-GaN Schottky diode proposed in this work is shown in Fig. 1. Starting from a GaN n^+ substrate with a doping concentration of 5×10^{19} cm^{-3}, a 5-μm-thick epitaxial layer with a donor doping level of 1×10^{16} cm^{-3} and a Pt metal layer, which acts as the anode region, are considered. The diode has been designed in order to perform a theoretical breakdown voltage close to 1400 V at room temperature.

Using the Silvaco TCAD 2D simulator [20], the device structure has been finely meshed and the metal/semiconductor and the n/n^+ interfaces have been accurately refined.

3. Physical models

The key physical models used in the simulation include the Shockley-Read-Hall (SRH) and Auger recombination processes, incomplete doping activation, impact ionization, bandgap temperature dependence, and carrier mobility as a function of both doping and temperature. The temperature dependence of the GaN bandgap [21] and intrinsic carrier concentration [22] are assumed in the forms of

$$E_g(T) = E_{g0} + 9.39\times10^{-4}\left(\frac{300^2}{300+772} - \frac{T^2}{T+772}\right), \qquad (1)$$

$$n_i(T) = 1.98\times10^{16}\times T^{3/2}\exp\left(-\frac{20488}{T}\right), \qquad (2)$$

where E_{g0} = 3.396 eV is the bandgap energy at T = 300 K.

Starting from the effective intrinsic carrier concentration, the Auger [23] and SRH [24] recombination rates are modeled using the standard expressions:

$$R_{Auger} = \left(C_p p + C_n n\right)\left(np - n_i^2\right), \qquad (3)$$

$$R_{SRH} = \frac{pn - n_i^2}{\tau_p\left[n + n_i\exp\left(\frac{E_{trap}}{kT}\right)\right] + \tau_n\left[p + n_i\exp\left(-\frac{E_{trap}}{kT}\right)\right]}, \qquad (4)$$

where $C_n = 1\times10^{-30}$ cm^{6}s^{-1} and $C_p = 1\times10^{-31}$ cm^{6}s^{-1} are the Auger coefficients, E_{trap} is the difference between the trap energy level and the intrinsic Fermi level, and τ_n and τ_p are the carrier lifetimes dependent on the doping level, as described by Scharfetter's relation [23]:

$$\tau_{n,p} = \frac{\tau_{0n,p}}{1+\left(\frac{N}{N_{n,p}^{SRH}}\right)^{\gamma_{n,p}}}. \quad (5)$$

Here, N is the total impurity concentration for a given device region, and $\tau_{0n,p} = 0.5$ ns, $N_{n,p}^{SRH} = 5\times10^{16}$ cm^{-3}, and $\gamma = 1$ are the reference parameters [22].

The electron and hole impact ionization rates, $\alpha_{n,p}$, which are defined as the number of electron-hole pairs generated by the carriers traveling a unit distance along the direction of the electric field, are modeled using the following empirical expression:

$$\alpha_{n,p} = a_{0n,p}\exp\left(-\frac{b_{0n,p}}{E}\right). \quad (6)$$

The coefficients a_0 and b_0 are listed in Table I.

Assuming the Fermi-Dirac statistics, the incomplete ionization of impurities can be expressed using [25]:

$$N_d^+ = \frac{N_d}{1+2\left(\frac{N_d}{N_C}\right)\exp\left(\frac{\Delta E_d}{kT}\right)}, \quad (7)$$

$$N_a^- = \frac{N_a}{1+4\left(\frac{N_a}{N_V}\right)\exp\left(\frac{\Delta E_a}{kT}\right)}, \quad (8)$$

where N_d and N_a are the substitutional n-type and p-type doping concentrations, ΔE_a and ΔE_d are the acceptor and donor energy levels (e.g., ΔE_d =16 meV for Si and ΔE_a= 175 meV for Mg), and N_C and N_V are the electron and hole densities of states varying with temperature, as given in Ref. 22.

$$N_C(T) = 2.3\times10^{18}\left(\frac{T}{300}\right)^{3/2} \quad (9)$$

$$N_V(T) = 4.6\times10^{19}\left(\frac{T}{300}\right)^{3/2} \quad (10)$$

Finally, to model the carrier mobilities, the Caughey-Thomas analytic model is used [26].

$$\mu_{n,p} = \mu_{\min_{n,p}} + \frac{\mu_{\max_{n,p}}\left(\frac{T}{300}\right)^{\alpha} - \mu_{\min_{n,p}}}{1+\left(\frac{T}{300}\right)^{\beta}\left(\frac{N_{tot}}{N_{ref}}\right)^{\gamma}} \qquad (11)$$

Here, N_{tot} is the local (total) concentration of the ionized impurities, and $\mu_{min\ n,p}$, $\mu_{max\ n,p}$, α, β, and γ are the GaN-specific model parameters summarized in Table II [27].

In addition, Canali's model [28] is used to model high field-dependent mobility.

$$\mu_{n,p}(E) = \mu_{0n,p}\left[1+\left(E\frac{\mu_{0n,p}}{v_{sat}}\right)^{\kappa_{n,p}}\right]^{-1/\kappa_{n,p}}, \qquad (12)$$

where $\mu_{0n,p}$ is the low electric field mobility and v_{sat} is the temperature-dependent saturation velocity given in Ref. 24:

$$v_{sat} = \frac{2.7\times10^{7}}{1+0.8\exp\left(\frac{T}{600}\right)} \quad . \qquad (13)$$

Note that the simulation models assumed in this work have also been used in other recent papers of ours focusing on several SiC-based devices and, in particular, Al-implanted 4H-SiC p^{+}-i-n diodes [29-32]. In those papers, the models with their specific material parameters were also validated by comparison with experimental results obtained in a wide range of currents and temperatures.

4. Results and discussion

4.1 Analysis of the current density - voltage - temperature characteristics

For a Schottky barrier diode with relatively low doping levels, we can assume that the current is due to thermionic emission, meaning electrons in the conduction band travel over the potential barrier but not through it. The relationship between the applied voltage and the current density is given in Refs. 33 and 34:

$$J = J_0 \exp\left(\frac{qV}{nkT}\right)\left[1 - \exp\left(-\frac{qV}{kT}\right)\right], \qquad (14)$$

where q is the elementary charge, T is the temperature in Kelvin, k is the Boltzmann constant, n is the ideality factor, and J_0 is the reverse saturation current density, which can be extracted by extrapolating the straight line of ln(J) to intercept the axis at zero voltage. The ideality factor n is generally higher than 1 and it is used to indicate the deviation of practical diodes from the ideal thermionic emission model. The saturation current of the Schottky barrier can be expressed as

$$J_0 = A^* T^2 \exp\left(-\frac{q\Phi_b}{kT} \right). \qquad (15)$$

Here, A^* is the effective Richardson constant, which is equal to 26.4 $Acm^{-2}K^{-2}$ for GaN [35] and Φ_b is the Schottky barrier height. Assuming a forward bias voltage $V > 3kT/q$ [36], the conventional diode equation can be considered in the form of

$$J = J_0 \exp\left(\frac{qV}{nkT} \right). \qquad (16)$$

The simulated J-V characteristics of the presented Pt/n-GaN Schottky diode for a wide range of currents and temperatures are shown in Fig. 2.

In Fig. 2(a), we can note two regions where the temperature-dependent forward J-V characteristics behave differently. At low and medium current levels ($V < 1.3$ V), where the dominant current conduction mechanism is thermionic emission, the curves tend to shift toward the left and then upward as the temperature increases. This behavior is mainly due to the temperature dependence of intrinsic carrier concentration as well as carrier lifetime and the increase in electron thermal energy. At a forward voltage bias close to 1.3 V, corresponding to a current density of about 400 Acm^{-2}, however, all the curves cross each other at the same point. Therefore, in the series resistance region ($V > 1.3$ V) in Fig. 2(a), a negative temperature coefficient of current is observed, as reported in Ref. 22, in which quite similar GaN-based Schottky rectifiers have been investigated. Assuming that the diode series resistance is dominated by the resistivity effect of the GaN regions underlying the anode contact, this current behavior can be explained considering that the electron mobility decrease with temperature increasingly limits the device current capabilities.

The diode reverse leakage current densities in the same range of temperatures are shown in Fig. 2(b). A very low current density of 2.12×10^{-19} Acm^{-2} at -100 V and T = 300 K is calculated. However, this value increases significantly with temperature, which is possibly caused by a decrease in Schottky barrier height owing to the image force at the highest reverse biases, making thermal field emission transportation mechanisms more important. The breakdown voltage is in excess of 1300 V at all temperatures, assuming a current density on the order of 1 $mAcm^{-2}$ as the threshold.

The values of Φ_b and n, in the temperature range considered, are shown in Fig. 3. These behaviors are calculated from the low voltage J-V characteristics in forward bias, before the curves become dominated by the series resistance and deviate from linearity.

Φ_b and n are temperature-dependent. In particular, with increasing temperature, the ideality factor n decreases from 2.315 at T = 300 K to 2.207 at T = 500 K, while the SBH Φ_b increases from 1.446 eV at T = 300 K to 1.465 eV at T = 500 K. The SBH at room temperature is lower than the ideal value of 1.540 eV estimated on the basis of the Schottky-Mott model. During the calculations, we assumed a homogenous barrier at the interface and we extracted the Schottky parameters from the Arrhenius plot of the activation energy $\ln(J_0/T^2)$ against q/kT using Eq. (15), as shown in Fig. 4.

As can be seen, the Arrhenius plot shows a straight line, where the effective Richardson constant is obtained from the line intercept with the activation energy axis, resulting in A^* = 10.24 $Acm^{-2}K^{-2}$. SBH is obtained from the line slope, providing Φ_b = 1.42 eV. Note that A^* is lower than the expected theoretical value of 26.4 $Acm^{-2}K^{-2}$.

The discrepancies observed in the temperature dependences of both Φ_b and n, as well as the lower value of A^*, have often been attributed to current transport mechanisms not following the ideal TE theory, because of the existence of barrier inhomogeneities unavoidable even in the most carefully fabricated devices [36-39]. Since the current transport across the metal/semiconductor interface is a temperature-activated process, at low temperatures, electrons can surmount low barriers and the current transport will be dominated by current flowing through patches of low SBH and having a large value of the ideality factor. Therefore, the ideality factor simply indicates the barrier uniformity and it increases in an inhomogeneous

barrier [40]. When temperature increases, more and more electrons have sufficient energy to surmount a higher barrier. Consequently, the dominant barrier height will increase with temperature and bias voltage. Different types of barrier distribution function at the interface have been reported in the literature [41-43]. In our study, we use Werner and Güttler's model [17] with the assumption of a Gaussian distribution $\rho(\Phi_b)$ of SBH, with the standard deviation σ_0 at an approximately mean $\overline{\Phi_{b0}}$ given as

$$\rho(\Phi_b) = \frac{1}{\sigma_0\sqrt{2\pi}} \exp\left[-\frac{\left(\Phi_b - \overline{\Phi_{b0}}\right)^2}{2\sigma_0^2}\right], \tag{17}$$

where the term $1/\sigma_0\sqrt{2\pi}$ is a normalization constant. Therefore, the total forward current density across the Schottky structure can be expressed as

$$J = \int_{-\infty}^{+\infty} j(\Phi_b, V)\rho(\Phi_b)\,d\Phi_b, \tag{18}$$

where $J(\Phi_b, V)$ is the amount of current density at the barrier height Φ_b and the bias voltage V on the basis of the ideal TE theory. Then, introducing $J(\Phi_b, V)$ and $\rho(\Phi_b)$ from Eqs. (14) and (17) into Eq. (18), and calculating the integration to obtain the current density across the Schottky barrier under forward bias, we can write

$$J = A^* T^2 \exp\left[-\frac{q}{kT}\left(\overline{\Phi_{b0}} - \frac{q\sigma_0^2}{2kT}\right)\right] \exp\left(\frac{qV}{n_{App}kT}\right)\left[1 - \exp\left(-\frac{qV}{kT}\right)\right], \tag{19}$$

$$J_0 = A^* T^2 \exp\left(-\frac{q\Phi_{b,App}}{kT}\right), \tag{20}$$

where n_{App} has to be considered as the apparent ideality factor and $\Phi_{b,App}$ is the apparent SBH. The comparison of Eq. (14) with Eq. (19) gives

$$\Phi_{b,App} = \overline{\Phi_{b0}} - \frac{q\sigma_0^2}{2kT}. \tag{21}$$

Werner and Güttler assume that the mean SBH is linearly bias-dependent because $\Phi_b = \overline{\Phi_{b0}} + \rho_2 V$, whereas the standard deviation σ has bias dependence in the form of $\sigma^2 - \sigma_0^2 = \rho_3 V$. Here, ρ_2 and ρ_3 are

temperature-independent voltage coefficients, which quantify the voltage deformation of barrier distribution. The expression of the apparent ideality factor n_{App} as a function of temperature is given by [17]

$$\frac{1}{n_{App}} - 1 = \rho_2 - \frac{q\rho_3}{2kT}. \tag{22}$$

The plot of $\Phi_{b,App}$ against $q/2kT$ in Fig. 5 shows a rather straight line as expected. The values of $\overline{\Phi_{b0}}$ and zero-bias standard deviation σ_0 are obtained from the intercept and the slope of the straight line as 1.48 eV and 0.047 V, respectively.

Likewise, the plot of the term (n^{-1}-1) against $q/2kT$ shows a straight line as shown in Fig. 6. The values of ρ_2 and ρ_3 are calculated from the intercept and slope of the reported straight line as -0.52 and 0.0026 V, respectively. Combining Eqs. (20) and (21), we obtain the modified activation energy expression as

$$\ln\left(\frac{J_0}{T^2}\right) - \frac{q^2\sigma_0^2}{2k^2T^2} = \ln\left(A^*\right) - \frac{q\overline{\Phi_{b0}}}{kT}. \tag{23}$$

The plot of $\ln(J_0 / T^2) - q^2\sigma_0^2 / 2k^2T^2$ as a function of q/kT should also be a straight line, according to Eq. (23), with a slope and intercept immediately giving $\overline{\Phi_{b0}}$ and A^*, respectively. Using the least-squares linear fitting for the obtained curve shown in Fig. 7, we obtain $\overline{\Phi_{b0}}$ = 1.49 eV and A^*= 28.22 Acm^{-2}K^{-2}. As can be seen, the value of $\overline{\Phi_{b0}}$ is almost the same as that extracted from Fig. 5. On the other hand, the value of A^*, obtained from the modified activation energy plot, is very close to the theoretical value of 26.4 Acm-^{2}K^{-2} for n-type GaN.

4.2 Analysis of an acceptor trap state effect

In this section, we discuss the effects of an acceptor trap concentration N_{tA} of 1×10^{16} cm^{-3}on the Pt/n-GaN Schottky diode *J-V* characteristics at four different trap energy levels. In more detail, we simulate the forward and reverse *J-V* characteristics firstly with the shallow trap level H2 (E_v+0.25 eV), then with the deep levels H1 (E_v+0.87 eV), H4 (E_v+1.19 eV), and H5 (E_v+1.76 eV), and finally in the presence of all

four trap levels H2, H1, H4, and H5, as shown in Fig. 8. The trap parameters used for the simulations are listed in Table III.

On the basis of the simulation results, it is evident that the presence of traps has a significant impact on the device forward-bias electrical characteristics, especially when the trap states are located at the deepest energy levels. In addition, the diode threshold voltage tends to increase.

On the other hand, it is obvious that the leakage currents of diode structures containing traps are smaller than those of trap-free devices and we can calculate a leakage current of 1.8×10^{-19} Acm^{-2} at -100 V when all trap levels are considered. The observed behaviors of current density, in both forward and reverse biases when the trap level becomes deeper, have to be mainly related to a reduction in GaN majority carrier concentration. To ensure this, the distribution of electron concentrations along the device structure, corresponding to each trap level in both forward and reverse biases, is shown in Fig. 9.

It is seen in Fig. 9 that the electron concentration considerably decreases in the GaN n^- region in both forward and reverse biases, especially for the deepest trap level H5 and when all trap levels are present, which is due to the important hole density generated by the ionized acceptor trap states.

The effects of acceptor trap states with different concentrations and energy levels on the diode ideality factor and Schottky barrier height are shown in Figs. 10 and 11, respectively. Figure 12 shows the effect of the existence of an acceptor trap density N_{tA} of 1×10^{16} cm^{-3} in GaN on the energy band diagram of the Pt/n-GaN Schottky diode for each of the following trap types (H2, H1, H4, and H5). In addition, in Fig. 12, the case in which all trap types are present at the same time with a total trap density of 4×10^{16} cm^{-3} is also reported. The ideality factor remains constant with the trap concentration at the shallow trap level H2 and increases at the deep trap level H5, as expected from the role of traps as recombination centers. Similarly, from Fig. 11, the Schottky barrier height increases with the increase in deep trap density and remains quite constant at the shallow trap level H2. On the other hand, it is clearly shown in Fig. 12 that SBH increases when the trap level becomes deeper and reaches a maximum of 1.52 when all trap types are present in GaN. This is an effect of displacement damage induced by energetic particle irradiation. The introduced traps

cause the corresponding reductions in conductivity, mobility, and minority carrier lifetime, meaning a reduction in the majority carrier density in GaN.

5. Conclusions

In this paper, a simulation study of the *J-V-T* characteristics of a Pt/n-GaN Schottky diode has been presented and the effects of shallow and deep acceptor trap levels with different densities into the GaN regions have been investigated. The ideality factor decreases and SBH increases with the increase in temperature. These behaviors have been interpreted on the basis of the TE theory assuming a GD of SBH. By plotting the apparent barrier height against $q/2kT$, the zero-bias mean value $\overline{\Phi_{b0}}$ and the standard deviation σ_0 have been determined to be 1.48 eV and 0.047 V, respectively. From the modified activation energy plot, practically the same value of $\overline{\Phi_{b0}}$ has been extracted, and an effective Richardson constant of 28.22 $Acm^{-2}K^{-2}$, which is very close to the theoretical value, has been calculated. The linearity of the modified activation energy plot and the closeness of the Richardson constant to its theoretical value verify the assumed GD of SBH.

We also found that the presence of acceptor trap levels in bulk GaN affect considerably the electrical characteristics of the diode. In addition, the ideality factor and SBH take high values for acceptor trap concentrations equal to and beyond 1×10^{16} cm^{-3}, especially for the deepest trap level H5 and when all trap levels are present, because of the important hole densities generated by the ionized acceptor trap states.

References

[1] G. Wang, K. Fu, C. S. Yao, D. Su, G. G. Zhang, J. Y. Wang, and M. Lu, Nucl. Instrum. Methods Phys. Res., Sect. A **663**, 10 (2012).

[2] M. S. P. Reddy, A. A. Kumar, and V. R. Reddy, Thin Solid Films **519**, 3844 (2011).

[3] L. C. Chen, C. Y. Hsu, W. H. Lan, and S. Y. Teng, Solid-State Electron. **47**, 1843 (2003).

[4] Y. K. Su, F. S. Juang, and M. H. Chen, Jpn. J. Appl. Phys. **42**, 2257 (2003).

[5] R. Werner, M. Reinhardt, M. Emmerling, A. Forchel, V. Harle, and A. Bazhenov, Physica E **7**, 915 (2000).

[6] K. J. Schoen, J. M. Woodall, J. A. Cooper, and M. R. Melloch, IEEE Trans. Electron Devices **45**, 1595 (1998).

[7] A. C. Schmitz, A. T. Ping, M. Asif Khan, Q. Chen, J. W. Yang, and I. Adesida, Semicond. Sci. Technol. **11**, 1464 (1996).

[8] J. D. Guo, M. S. Feng, R. J. Guo, F. M. Pan, and C. Y. Chang, Appl. Phys. Lett. **67**, 2657 (1995).

[9] L. Wang, M. I. Nathan, T. H. Lim, M. A. Khan, and Q. Chen, Appl. Phys. Lett. **68**, 1267 (1996).

[10] Y. Kribes, I. Harrison, B. Tuck, T. S. Cheng, and C. T. Foxon, Semicond. Sci. Technol. **12**, 913 (1997).

[11] P. Hacke, T. Detchprohm, K. Hiramatsu, and N. Sawaki, Appl. Phys. Lett. **63**, 2676 (1993).

[12] J. D. Guo, F. M. Pan, M. S. Feng, R. J. Guo, P. F. Chow, and C. Y. Chang, J. Appl. Phys. **80**, 1623 (1996).

[13] E. V. Kalinina, N. J. Kurnestov, V. A. Dmitreiev, K. G. Irvine, and C. H. Carter, J. Electron. Mater. **25**, 831 (1996).

[14] M. T. Hirsch, K. J. Duxstad, and E. E. Haller, Electron. Lett. **33**, 95 (1997).

[15] H. Morkoç, *Handbook of Nitride Semiconductors and Devices: Electronic and Optical Processes in Nitrides* (Wiley-VCH, Weinheim, 2008) p. 50.

[16] R. T. Tung, Phys. Rev. B **45**, 13509 (1992).

[17] J. H. Werner and H. H. Güttler, J. Appl. Phys. **69**, 1522 (1991).

[18] M. Moll, Nucl. Instrum. Methods Phys. Res., Sect. A **546**, 202 (2006).

[19] L. Ling, J. G. Ma, Y. R. Cao, J. C. Zhang, W. Zhang, L. Li, S. R. Xu, X. H. Ma, X. T. Ren, and Y. Hao, Microelectron. Reliab. **51**, 2168 (2011).

[20] Silvaco Atlas User's Manual (2013).

[21] H. Teisseyre, P. Perlin, T. Suski, I. Grzegory, S. Porowski, and J. Jun, J. Appl. Phys. **76**, 2429 (1994).

[22] K. H. Baik, Y. Irokawa, F. Ren, S. J. Pearton, and S. S. Park, Solid-State Electron. **47**, 1533 (2003).

[23] S. J. Pearton, C. R. Abernathy, and F. Ren, *Gallium Nitride Processing for Electronics, Sensors and Spintronics* (Springer, London, 2006) p. 186.

[24] W. Shockley and W. T. Read, Phys. Rev. **87**, 835 (1952).

[25] M. Razeghi and M. Henini, *Optoelectronic Devices: III-Nitrides* (Elsevier, Amsterdam, 2004) p. 327.

[26] D. Caughey and R. Thomas, Proc. IEEE **52**, 2192 (1967).

[27] T. T. Mnatsakanov, M. E. Levinshtein, L. I. Pomortseva, S. N. Yurkov, G. S. Simin, and M. A. Khan, Solid-State Electron. **47**, 111 (2003).

[28] C. Canali, G. Majni, R. Minder, and G. Ottaviani, IEEE Trans. Electron Devices **22**, 1045 (1975).

[29] M. L. Megherbi, F. Pezzimenti, L. Dehimi, S. Rao, and F. G. Della Corte, Solid-State Electron. **109**, 12 (2015).

[30] F. Pezzimenti, IEEE Trans. Electron Devices **60**, 1404 (2013).

[31] S. Bellone, F. G. Della Corte, L. Freda Albanese, and F. Pezzimenti, IEEE Trans. Power Electron. **26**, 2835 (2011).

[32] F. Pezzimenti, F. G. Della Corte, and R. Nipoti, Microelectron. J. **39**, 1594 (2008).

[33] S. M. Sze and K. K. Ng, *Physics of Semiconductor Devices* (Wiley, Hoboken, NJ, 2006) 3rd ed., p. 157.

[34] H. C. Card and E. H. Rhoderick, J. Phys. D **4**, 1589 (1971).

[35] M. Drechsler, D. M. Hoffman, B. K. Mayer, T. Detchprohm, H. Amano, and I. Akasaki, Jpn. J. Appl. Phys. **34**, 1178 (1995).

[36] S. Gholami and M. Khakbaz, Int. J. Electr. Comput. Energetic Electron. Commun. Eng. **5**, 1280 (2011).

[37] H. K. Henisch, *Semiconductor Contacts* (Oxford University Press, Oxford, U.K., 1984) p. 123.

[38] S. Zhu, R. L. Van Meirhaeghe, C. Detavernier, G. P. Ru, B. Z. Li, and F. Cardon, Solid-State Commun. **112**, 611 (1999).

[39] S. Chand and J. Kumar, J. Appl. Phys. **82**, 5005 (1997).

[40] S. Zhu, R. L. Van Meirhaeghe, S. Forment, G. P. Ru, X. P. Qu, and B. Z. Li, Solid-State Electron. **48**, 1205 (2004).

[41] Y. P. Song, R. L. Van Meirhaeghe, W. H. Laflere, and F. Cardon, Solid-State Electron. **29**, 633 (1986).

[42] P. G. Mc Cafferty, A. Sellai, P. Dawson, and H. Elabd, Solid-State Electron. **39**, 583 (1996).

[43] Zs. J. Horváth, Proc. Int. Conf. Microelectronics, 1992, p. 453.

[44] Y. Tokuda, Proc. Int. Conf. Compound Semiconductor Manufacturing Technology, 2014, p. 19.

Fig. 1. Pt/n-GaN Schottky diode schematic cross section (plot not in scale).

Fig. 2. Simulated *J-V* characteristics of the Pt/n-GaN Schottky diode in the 300-500 K temperature range. (a) Forward bias. Inset: forward *J-V* characteristics in linear scale. (b) Reverse bias.

Fig. 3. Ideality factor and SBH extracted from the forward *J-V* characteristics of the Pt/n-GaN Schottky diode in the 300-500 K temperature range.

Fig. 4. Arrhenius plot of the activation energy $\ln(J_0/T^2)$ *vs* q/kT.

Fig. 5. $\Phi_{b,App}$ *vs* $q/2kT$ according to a GD of SBH.

Fig. 6. $(n^{-1}-1)$ *vs* $q/2kT$ according to a GD of SBH.

Fig. 7. Modified activation energy plot of $\ln(J_0 / T^2) - q^2\sigma_0^2 / 2k^2T^2$ *vs* q/kT according to a GD of SBH.

Fig. 8. Simulated *J-V* characteristics of the Pt/n-GaN Schottky diode introducing the H2, H1, H4, and H5 trap energy levels at $T = 300$ K. (a) Forward bias. (b) Reverse bias. Inset: magnified view of the reverse *J-V* characteristics up to -4 V.

Fig. 9. Electron concentration along the Pt/n-GaN structure at different trap energy levels at $T = 300$ K. (a) Forward bias. (b) Reverse bias.

Fig. 10. Ideality factor as a function of acceptor trap state density at $T = 300$ K. Inset: magnified view of the ideality factor in the 2.25-2.65 range.

Fig. 11. Schottky barrier height as a function of acceptor trap state density at $T = 300$ K. Inset: magnified view of SBH in the 1.445-1.456 eV range.

Fig. 12. Energy band diagram of Pt/n-GaN Schottky diode with an acceptor trap density N_{tA} of 1×10^{16} cm^{-3} for each acceptor trap level at $T = 300$ K.

Table I. GaN impact ionization parameters [22].

Carrier	a_0 (cm^{-1})	b_0 (Vcm^{-1})
Electron	2.41×10^{8}	3.40×10^{7}
Hole	5.41×10^{6}	1.96×10^{7}

Table II. GaN carrier mobility parameters.

Carrier	μ_{max} (cm²V^{-1}s^{-1})	μ_{min} (cm²V^{-1} s^{-1})	N_{ref} (cm^{-3})	α	β	γ
Electron	1418	55	2×10^{17}	-2	-3.8	1
Hole	175	30	3×10^{17}	-5	-3.7	2

Table III. Trap simulation parameters [44].

Trap level	Activation energy (eV)	Density (cm^{-3})	Electron capture cross section (cm²)	Hole capture cross section (cm²)
H2	0.25	1×10^{16}	1.7×10^{-17}	1.7×10^{-16}
H1	0.87	1×10^{16}	7.4×10^{-14}	7.4×10^{-13}
H4	1.19	1×10^{16}	2.3×10^{-15}	2.3×10^{-14}
H5	1.76	1×10^{16}	1.2×10^{-12}	1.2×10^{-11}

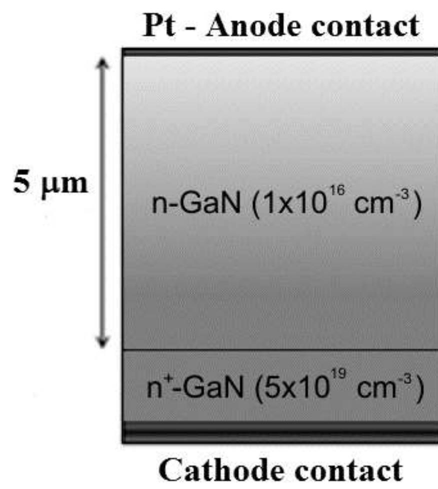

Figure 1

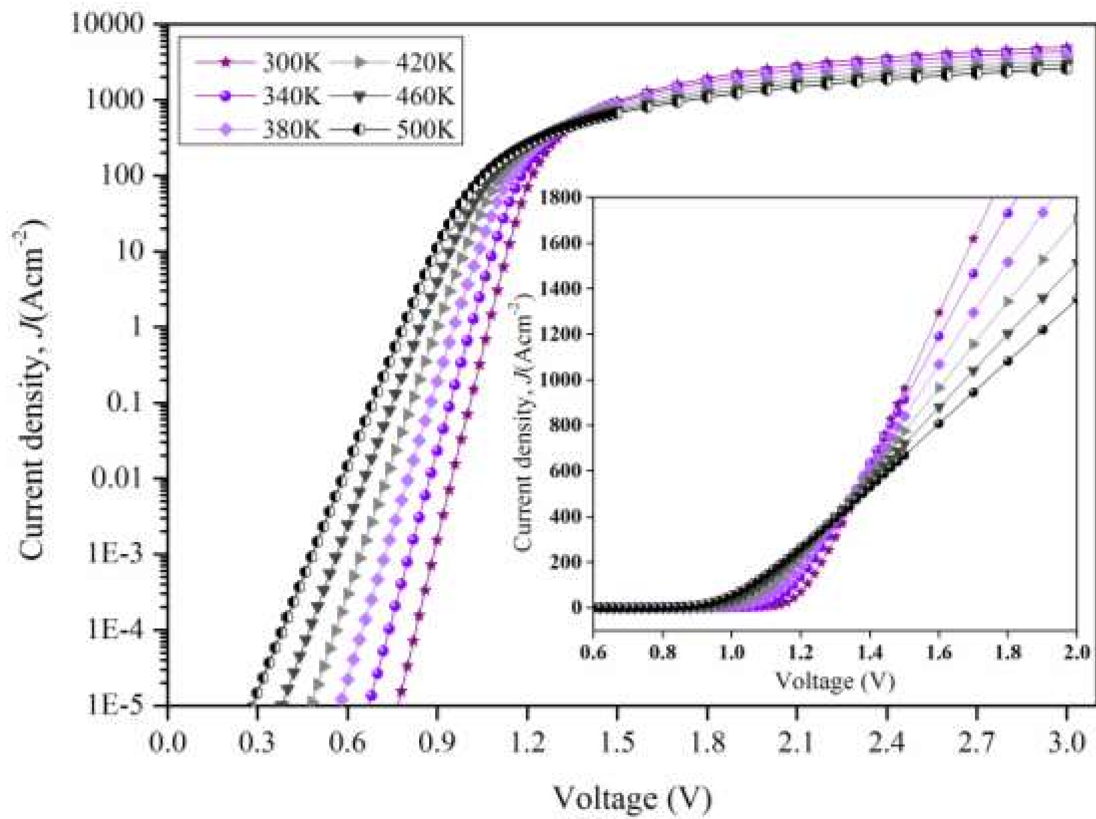

Figure 2(a)

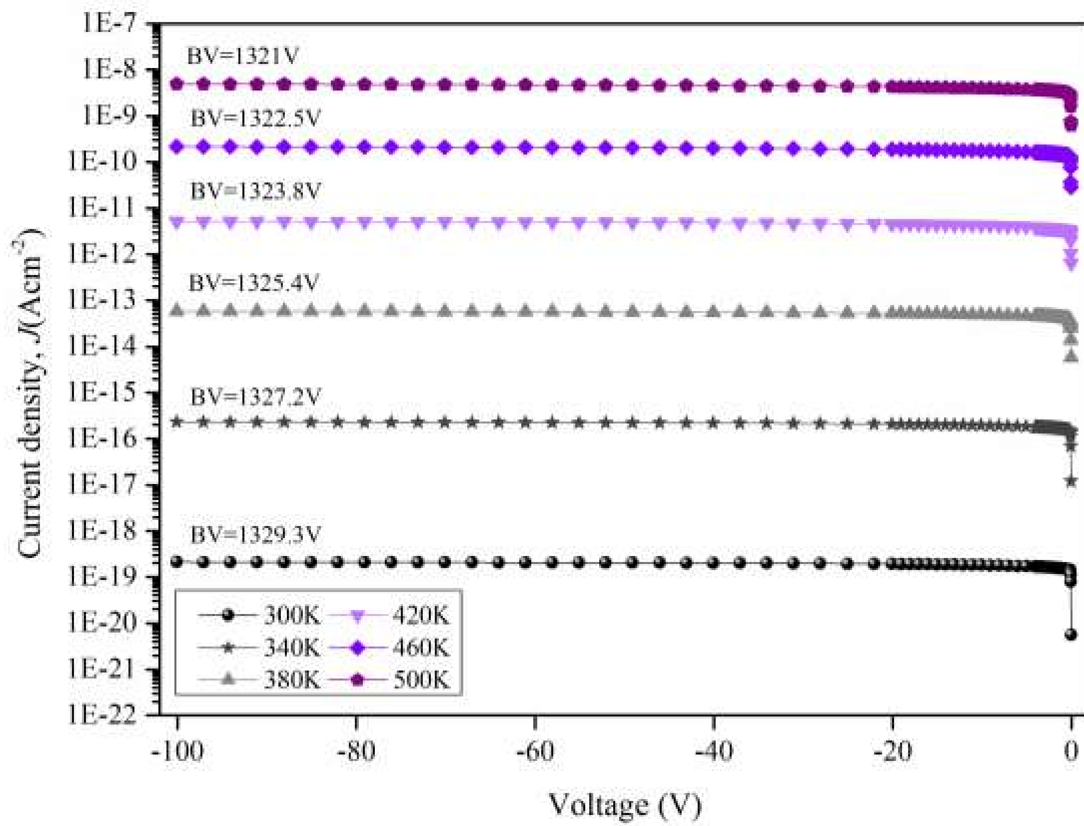

Figure 2(b)

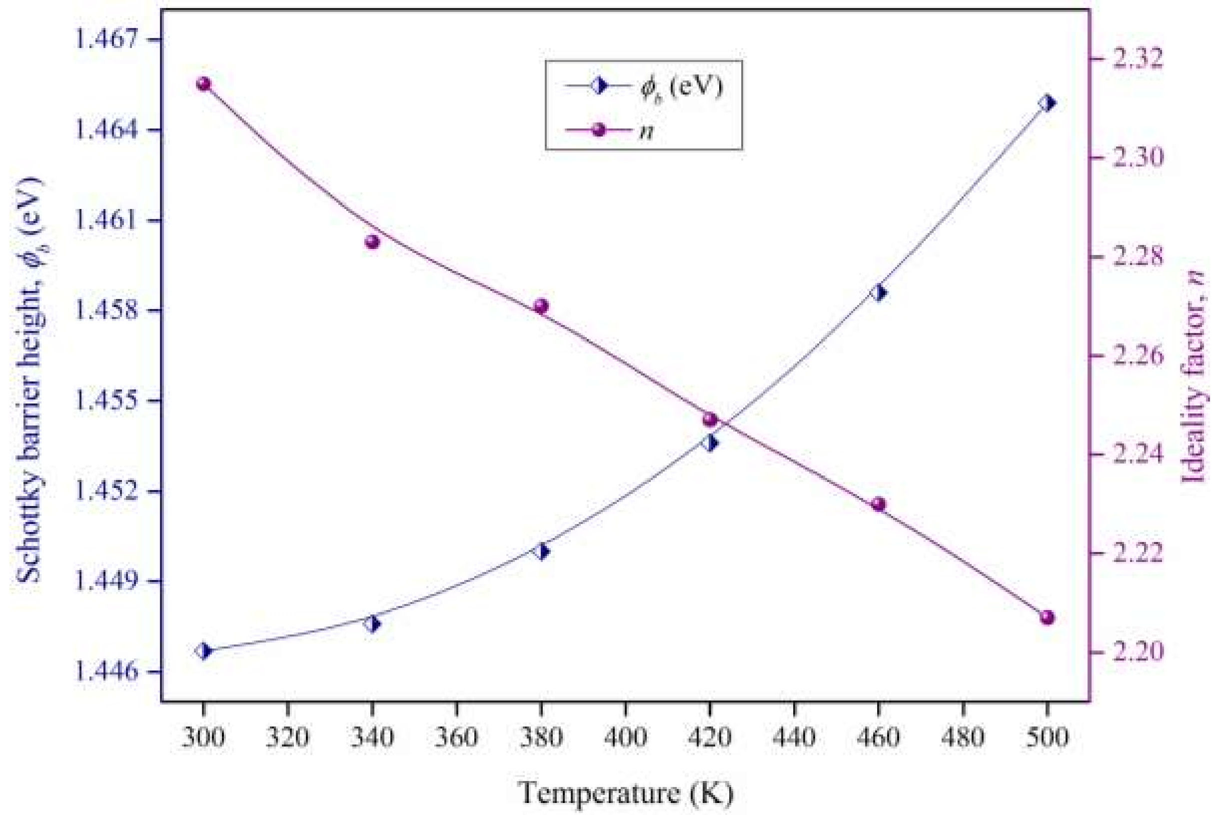

Figure 3

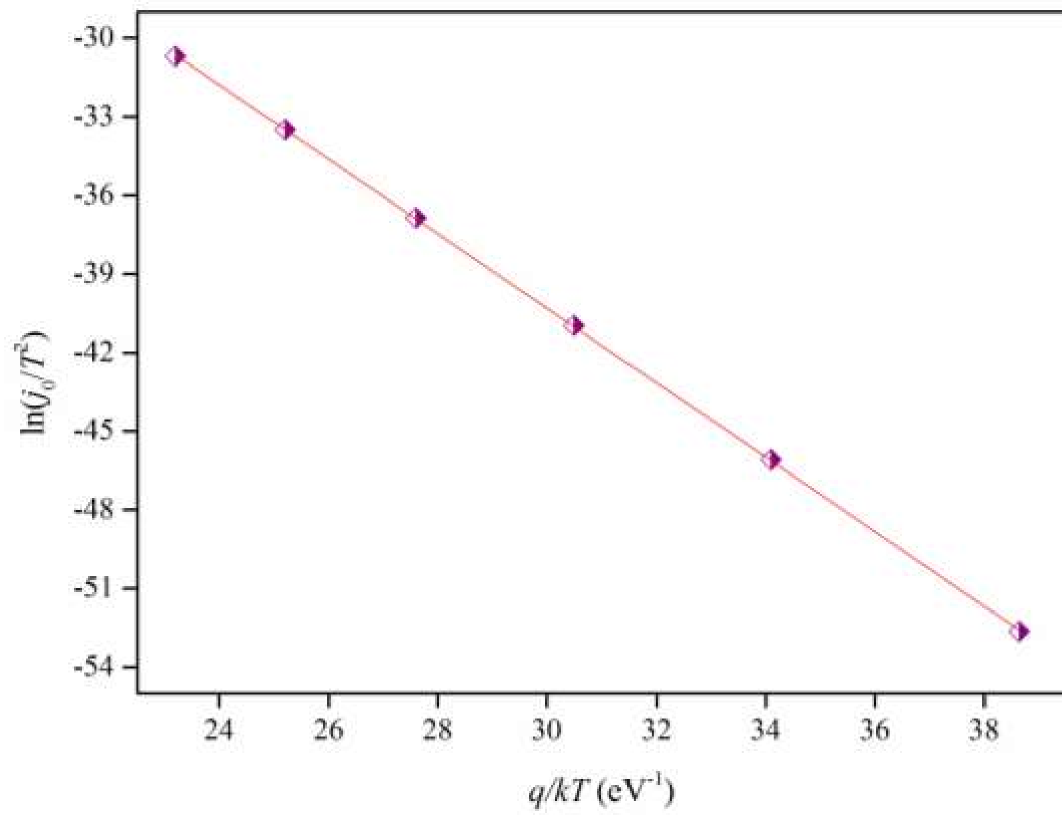

Figure 4

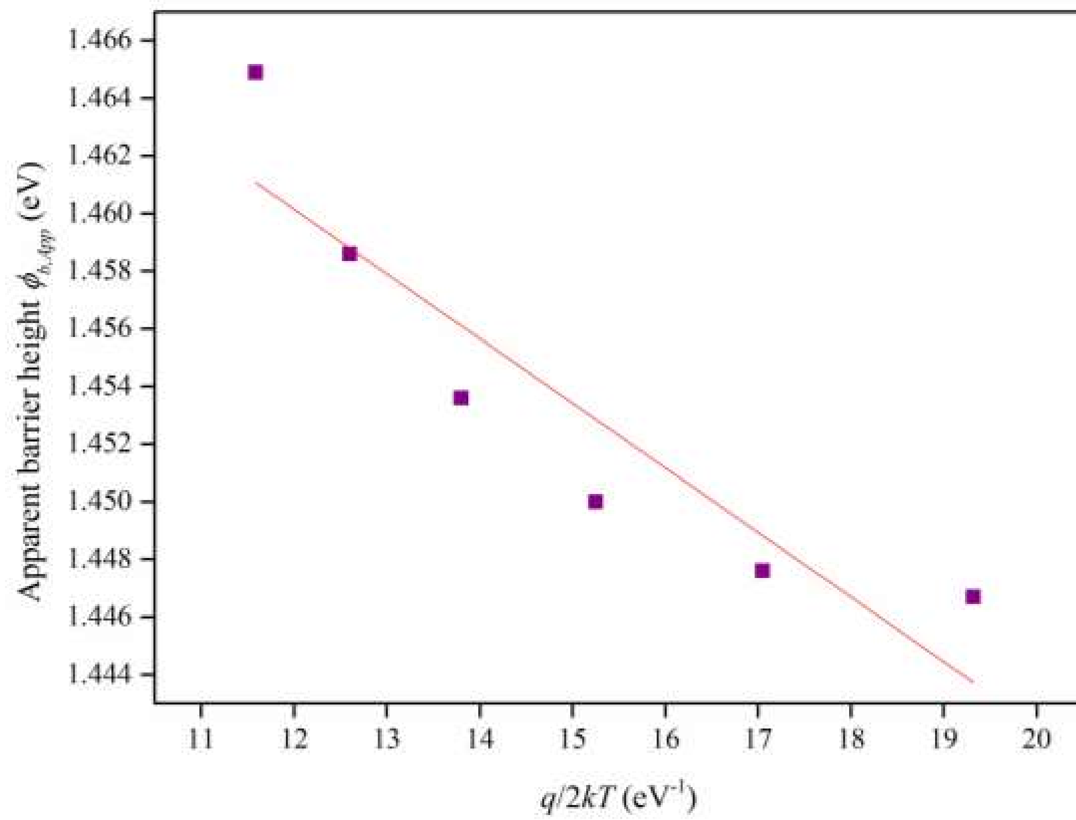

Figure 5

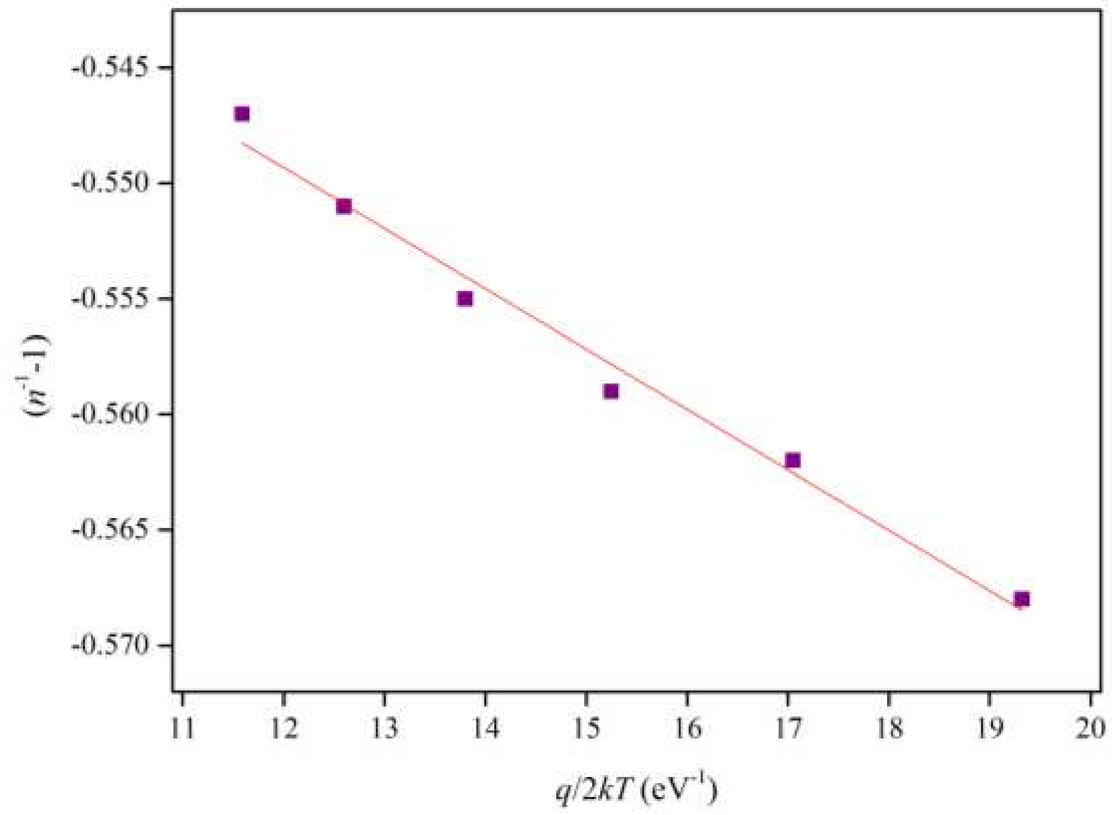

Figure 6

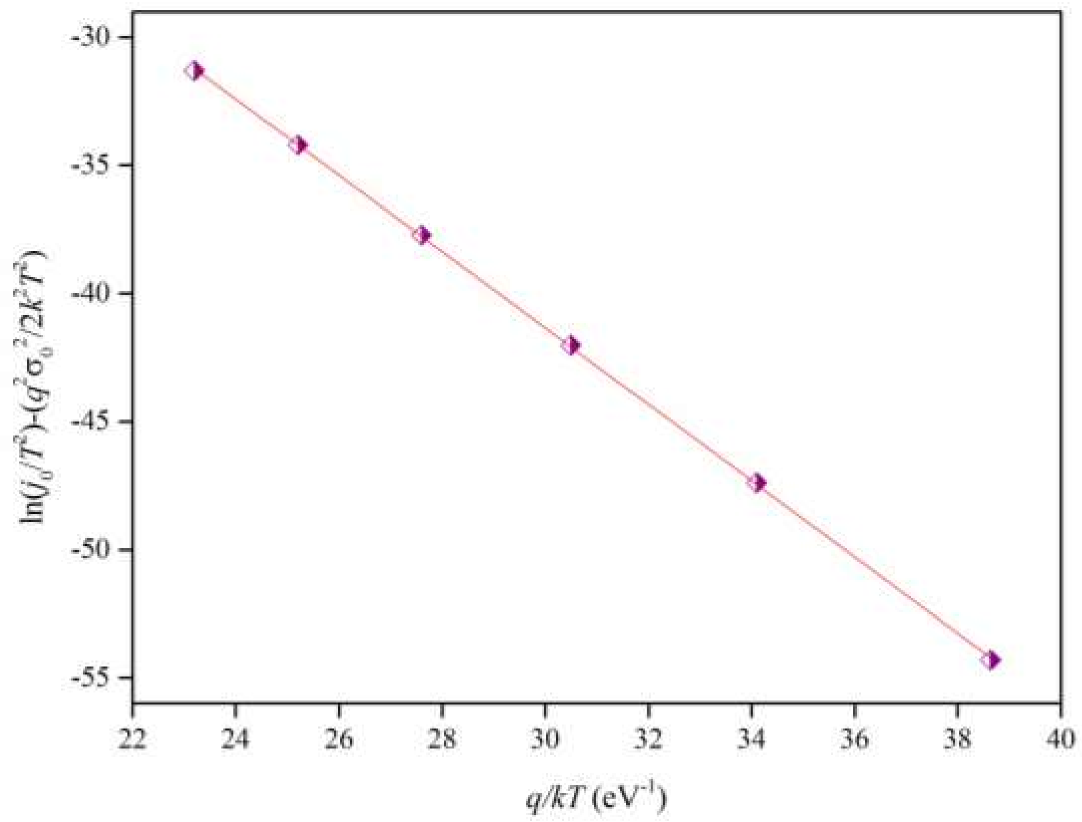

Figure 7

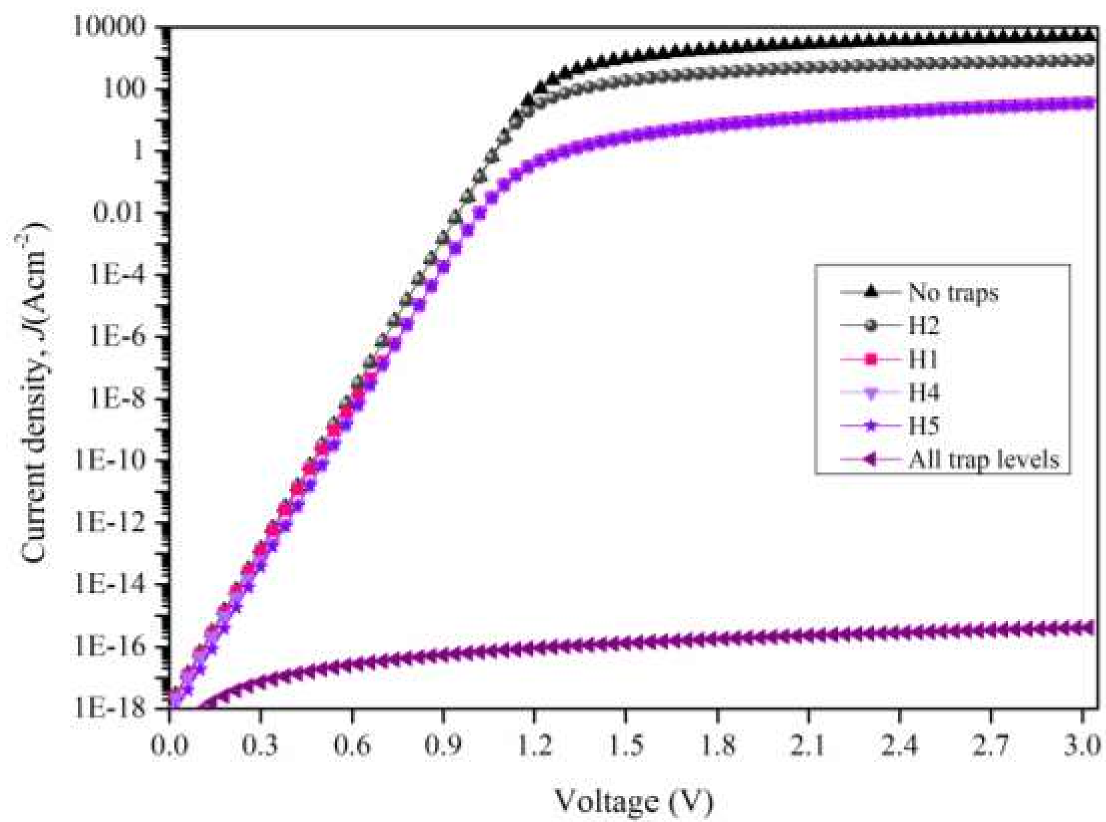

Figure 8(a)

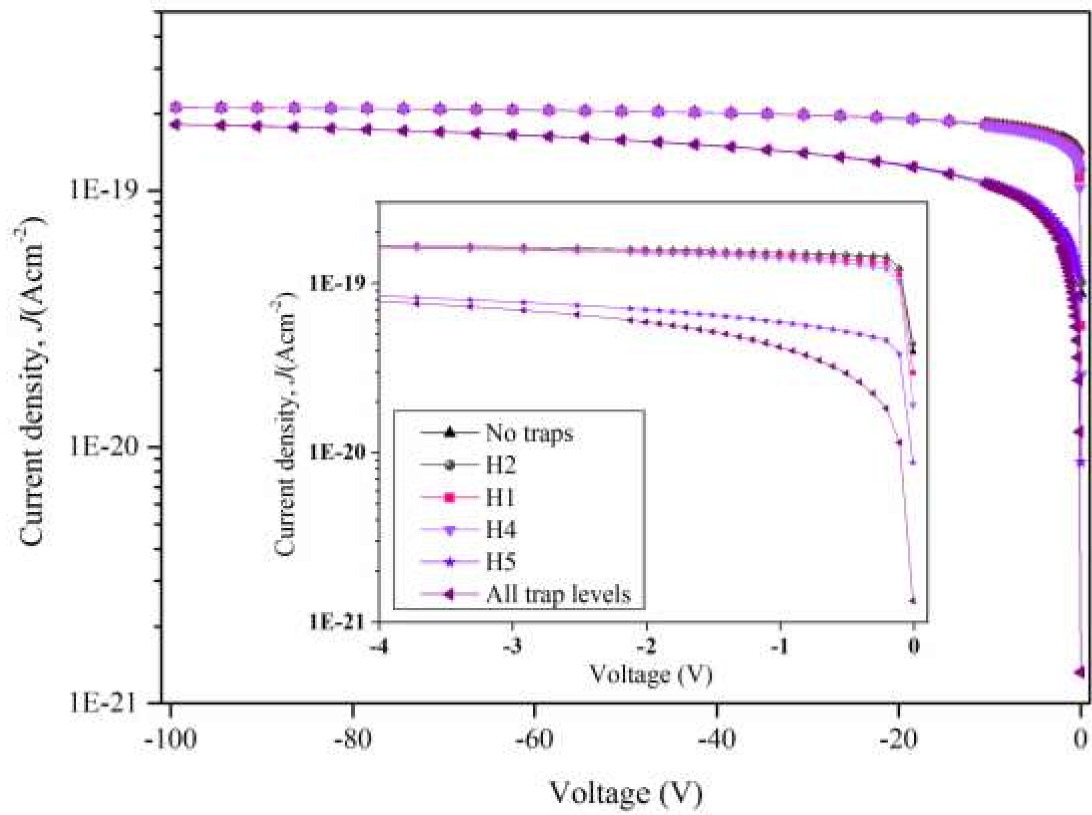

Figure 8(b)

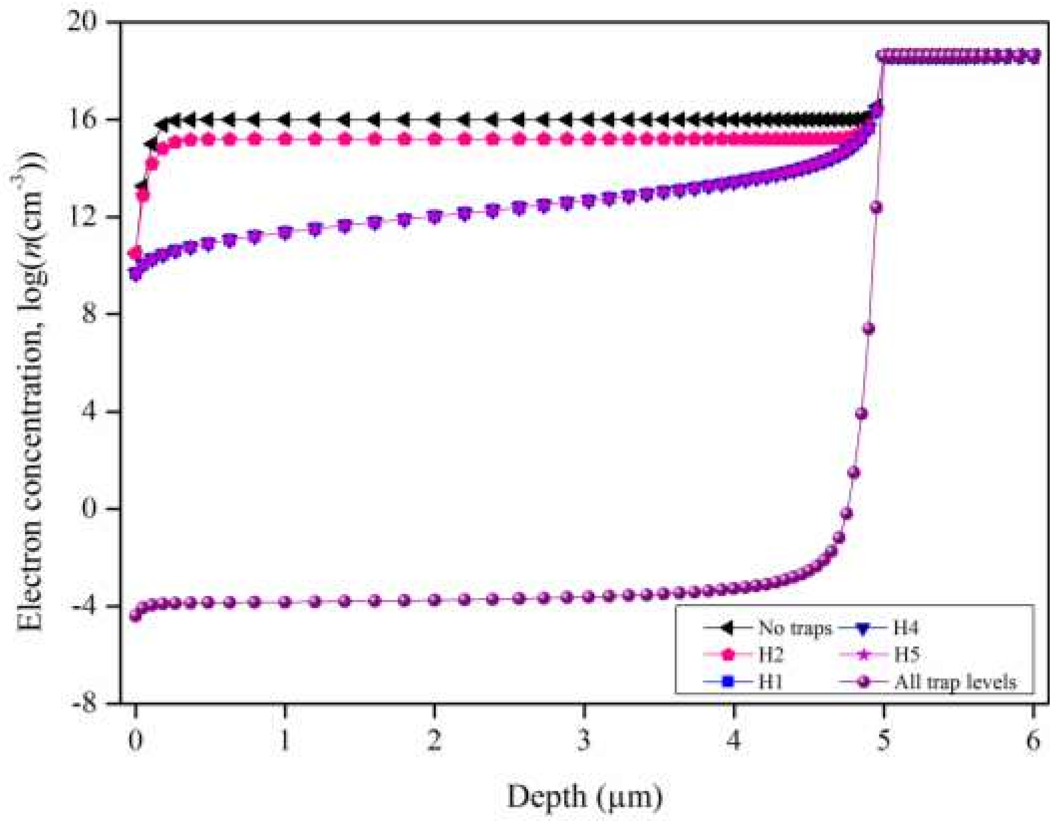

Figure 9(a)

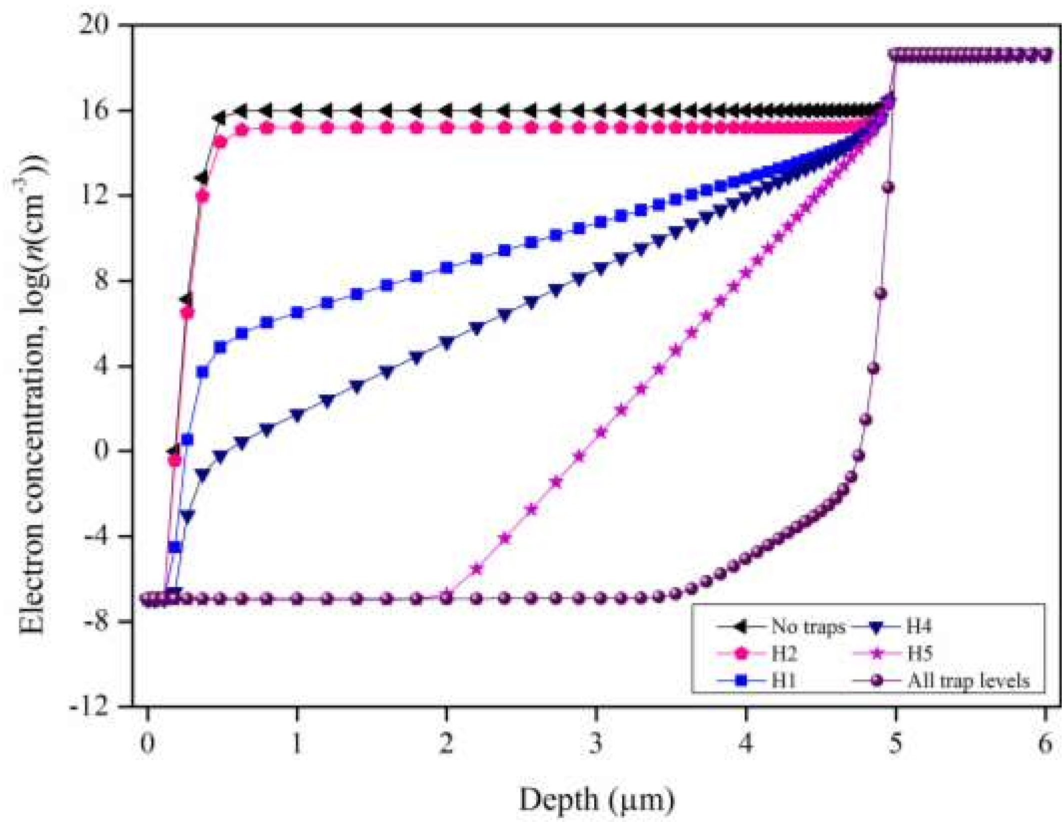

Figure 9(b)

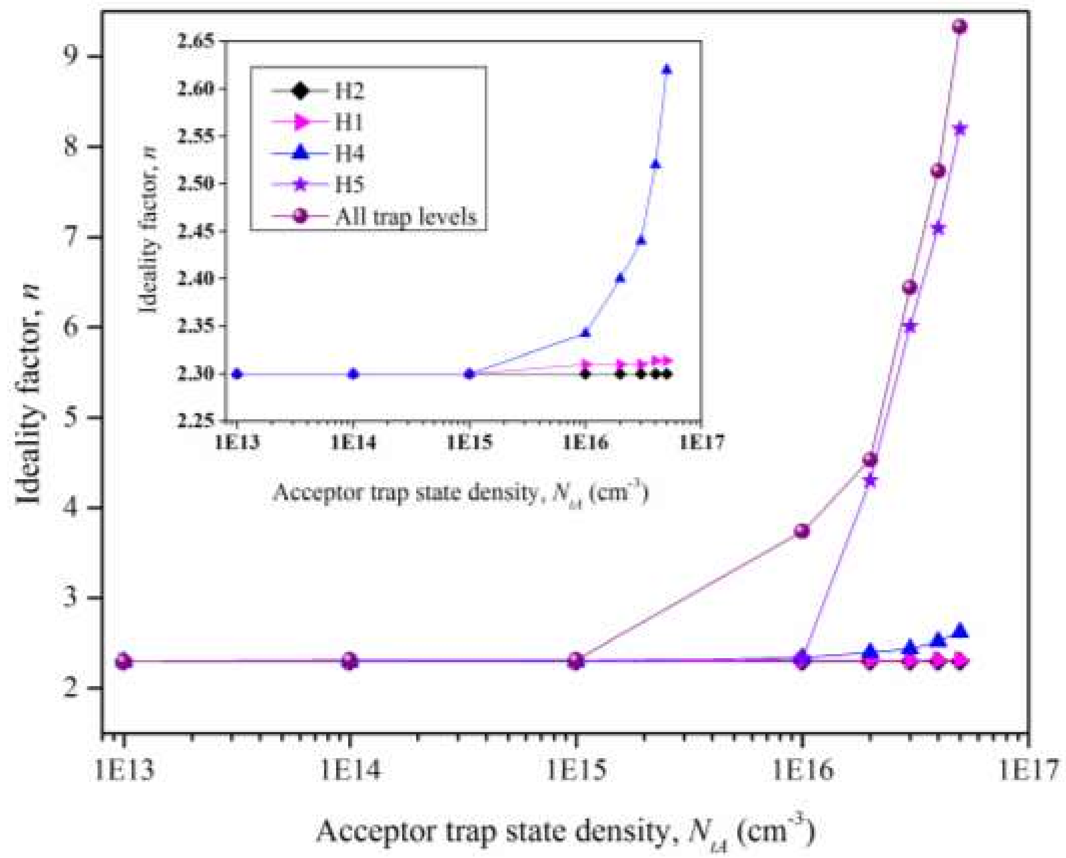

Figure 10

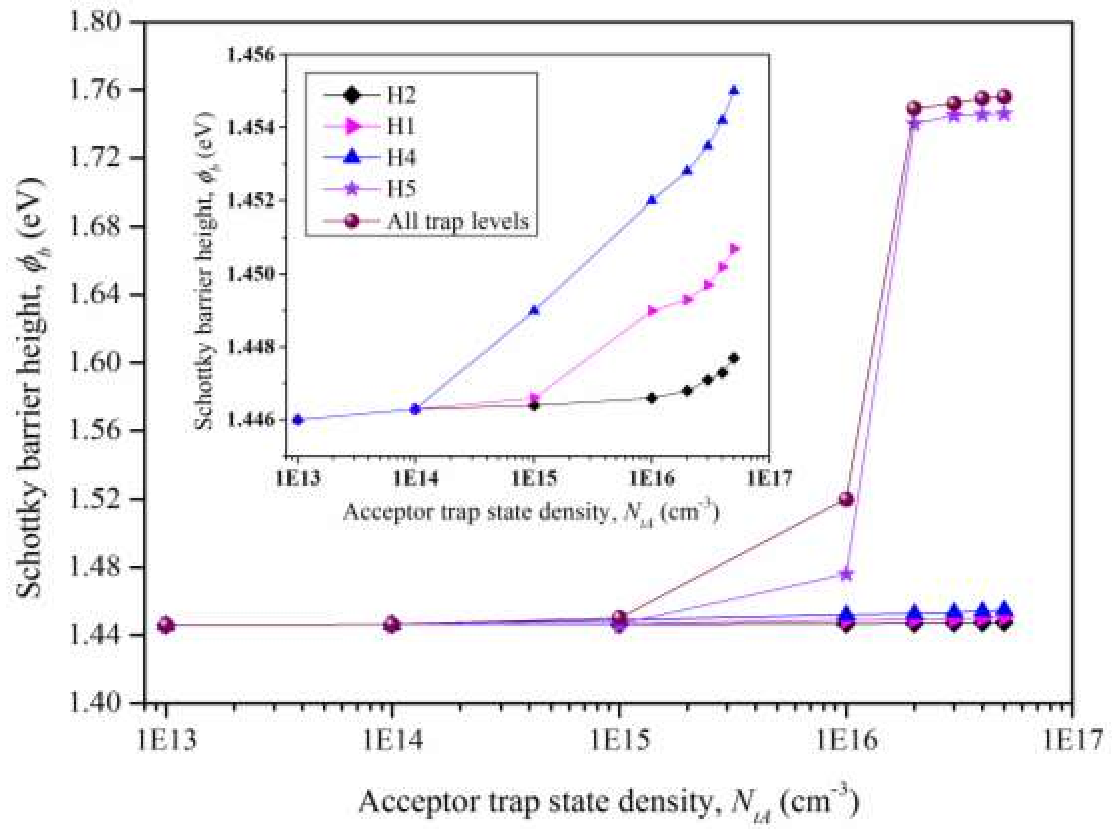

Figure 11

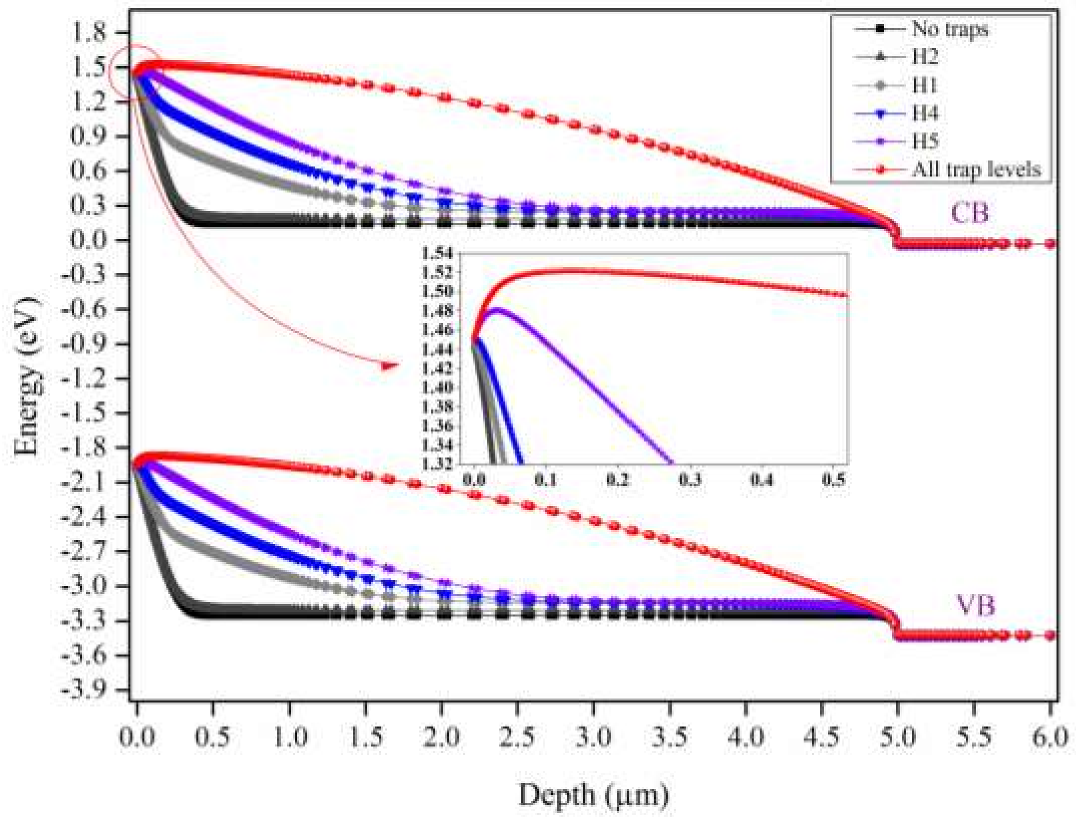

Figure 12